Numerical optimisation and recombination effects on the vertical-tunnel-junction (VTJ) GaAs solar cell up to 10,000 suns

Celia Outes, Eduardo F. Fernández, Natalia Seoane, Florencia Almonacid and Antonio J. García-Loureiro

Version: accepted article

Numerical optimisation and recombination effects on the vertical-tunnel-junction (VTJ) GaAs solar cell up to 10000 suns

Celia Outes[1]*, Eduardo F. Fernández[1]**, Natalia Seoane[2], Florencia Almonacid[1] and Antonio J. García-Loureiro[2]

[1]Centro de Estudios Avanzados en Ciencias de la Tierra, Energía y Medio Ambiente, University of Jaén, Spain

[2]Centro Singular de Investigación en Tecnoloxías Intelixentes, University of Santiago de Compostela, Spain

*corresponding author: coutes@ujaen.es

**corresponding author: eduardo.fernandez@ujaen.es

Abstract. Ultra-high concentrator photovoltaic systems (UHCPV), usually referred to CPV systems exceeding 1000 suns, are signalled as one of the most promising research avenues to produce a new generation of high-efficiency and low-cost CPV systems. However, the structure of current concentrator solar cells prevents their development due to the unavoidable series resistance losses at such elevated concentration ratios. In this work, we investigate the performance of the so-called vertical-tunnel-junction (VTJ), recently introduced by the authors, by using advance TCAD. In particular, we carry out an optimisation procedure of the key parameters that affect its performance and conduct a deep investigation of the impact of the main recombination mechanisms and of sun concentration up to 10000 suns. The results indicate that the performance of the novel structure is not significantly affected by these two factors. A record efficiency of 32.2 % at 10000 suns has been found. This represents a promising way to obtain state-of-the-art efficiencies above 30 % for single-band-gap cells, and offers a new route towards the development of competitive CPV systems operating at ultra-high concentration fluxes.

Keywords*: vertical solar cells, series resistance, gallium arsenide (GaAs), tunnel diode, concentrator photovoltaics*

1. Introduction

Concentrator photovoltaic (CPV) technology, usually with concentration factors (C_{ratio}) within 300-1100 suns, has achieved the highest efficiencies (η), >40 %, among all the PV technologies (Pérez-Higueras, et al., 2018). In addition, these systems have demonstrated a noteworthy capacity to produce high energy yields and to reduce the cost of electricity at locations with high solar energy resource (Fernández, et al., 2016; Kamath, et al., 2019). However, despite the remarkable progress and high η of commercial developments (i.e. >40 %, >30 % and >25 % at cell, module and system levels), there are no systems yet able to compete with the prices of conventional non-concentrating PVs (e.g. c-Si, p-Si, CdTe, CIGS, etc.). As a consequence, further efforts are still needed to lower their cost and improve their performance to compete with the classical flat PV technologies (Talavera, et al., 2016; Talavera, et al., 2017). In any case, as is also signalled by several authors, there is still room for huge technological improvements to increase the competitiveness of the technology (Wiesenfarth, et al., 2018).

Ultra-high CPV systems (UHCPV) with C_{ratio} far above 1000 suns is considered as one of the most promising research avenues to obtain high-efficiency and low-cost new generation CPV systems (Algora & Rey-Stolle, 2012). This can be explained considering that 1) the theoretical η of solar cells grows with C_{ratio} and 2) the amount of expensive semiconductor material is drastically reduced. Bearing this in mind, several efforts are being conducted by the community to develop a) solar cells with η peaking at UH levels (Ochoa, et al., 2016; Barrigón, et al., 2014; Paquette, et al., 2016), b) optical designs able to reach UH levels with an adequate optical performance (Ferrer-Rodríguez, et al., 2016; Shanks, et al., 2018) and c) thermal mechanisms able to remove or/and exploit the extreme heat waste produced by the cells at such elevated C_{ratio} (Vossier, et al., 2018; Valera, et al., 2019; Rodrigo, et al., 2019). The most relevant constraint to develop suitable UHCPV systems is related to the concentrator solar cells. Nowadays, CPV systems are largely based on multi-junction (MJ) horizontal structures made up of multiple III-V semiconductors with various energy gaps (E_G) (Cotal, et al., 2009; Theristis & O'Donovan, 2015). These cells incorporate only two electrical terminals, located on the top and the back. Consequently, there is an unavoidable trade-off between the shadowing of the front metal-grid pattern and the series resistance (R_s). This seems to limit the developing of MJ cells with η peaking at UH levels no matter how the top-metal pattern is designed or how much the cell area, so the current, is reduced (Paquette, et al., 2016). Indeed, according to the last η tables, it has not yet been possible to develop MJ cells with η peaking at C_{ratio} > 1000 suns based on current horizontal configurations (Green, 2020). This crucial drawback prevents the development of competitive UHCPV systems.

Vertical-multi-junction (VMJ) cells offer a straightforward solution to eliminate the R_s limitations of current architectures. These cells consist of a series connection of multiple subcells with the metallic contacts located on the laterals (Xing, 2013; Segev & Kribus, 2013; Gover & Stella, 1974). This way, it is possible to develop cells with low current densities, due to the large cross section of the current, and low R_s values, and therefore, to develop cells optimised for UH fluxes (Sater & Sater, 2002), (Tyukhov & Vasilev, 1995). On the other hand, nowadays, VMJ cells are limited to indirect band-gap materials with high carrier diffusion lengths (L), around 100-300 µm (Pozner, et al., 2011). This limitation is imposed by the fact that direct band-gap materials present much lower L, usually 1-5 µm. This would imply the series connection of approximately 200-1000 VMJ cells for achieving a solar cell side of 1 mm by using lateral metallic contacts. This manufacturing constraint is verified considering that, to the date, only silicon (Si) based VMJ solar cells have been developed (Xing, et al., 2015). Consequently, it is not possible to select the most convenient semiconductor materials to optimise the absorption of the spectrum. So, although the low R_s does not limit the performance of VMJ cells with C_{ratio}, the poor semiconductor selection prevents the development of high-efficiency multi-band-gap structures with an optimal absorption of the spectral irradiance (Braun, et al., 2012).

This work is focused on the optimisation and detailed performance evaluation of a novel vertical solar cell structure recently introduced by the authors in a short communication (Fernández, et al., 2019). This early design opened the way to either use direct or indirect band-gap semiconductors. Hence, it is possible to select the appropriate E_G for each particular application. In the present investigation, we carry out an optimisation procedure of the key parameters in order to investigate the expected maximum η of the new structure for the case of a single-band structure. In addition, we conduct a deep investigation of the effect of the main recombination mechanisms and C_{ratio} on the performance of the device. The results of this work are fundamental to fully understand and evaluate the potential of this promising device to produce a new generation of competitive

CPV systems operating at state-of-the-art concentration factors. Bearing this in mind, this paper represents one of the first efforts towards the design of a novel ultra-efficient concentrator solar cell, which is expected to serve as a key guideline for future work concerning its manufacturing and characterization.

This paper is organized as follows. In section 2, the structure of the device under consideration is described, and the simulation procedure used presented. After that, in section 3, the recombination mechanisms under scrutiny are briefly introduced. The optimisation of the solar cell investigated is discussed in section 4, and the numerical results of this optimised design presented in section 5. Finally, the main conclusions are summarized in section 6.

2. Device structure and simulation technique

The device investigated in this article is an optimisation of a novel structure recently proposed by the authors based on gallium arsenide (GaAs) (Fernández, et al., 2019). The elementary unit of the so-called vertical-tunnel-junction (VTJ) cell is made up of two identical subcells, with four layers each one, joined by a tunnel junction (TJ), as shown in Fig. 1. As in our early investigation, gallium arsenide (GaAs) has also been considered due to its ability for achieving high conversion efficiencies. In this structure, the anode and cathode are placed laterally. It is also worth mentioning that, as in our previous design, it is possible to increase the area of the cell exposed to the light by connecting multiple VTJs using TJs. In this sense, it is important to note that cell sides $\approx<$ 0.5 mm are desirable for developing UHCPV systems in order to facilitate the heat dissipation and to reduce the cell-to-module losses (Ritou, et al., 2018). These low cell areas are also key to limit the number of TJs of the total VTJ structure in order to facilitate the fabrication of the device.

At this stage, the width and doping values of the p^+ and n^+-layers remain fixed during the whole study because these layers were adjusted to the width and doping of the tunnel junction. The TJ consists of a GaAs n+/p+ structure, both layers having a 25 nm width and a doping of $7 \cdot 10^{19}$ cm^{-3}. This element has been simulated by including direct and trap-assisted tunnelling models, as previously used by other authors (García, et al., 2012). Regarding the p^+ and n^+-layers, they have a 0.07 μm width and constant doping value of $5 \cdot 10^{19}$ cm^{-3}. The width and doping of the p and n layers will be optimised in the next section for a specific C_{ratio} of 4000 suns. This C_{ratio} has been considered since recent investigations indicate the feasibility to develop UHCPV modules with sufficient optical and thermal performance at C_{ratio} around this value (Shanks, et al., 2018; Ferrer-Rodriguez, et al., 2020). These layers have been selected in the optimisation procedure since our preliminary simulations have proven that they are the most relevant to increase the final η of the device.

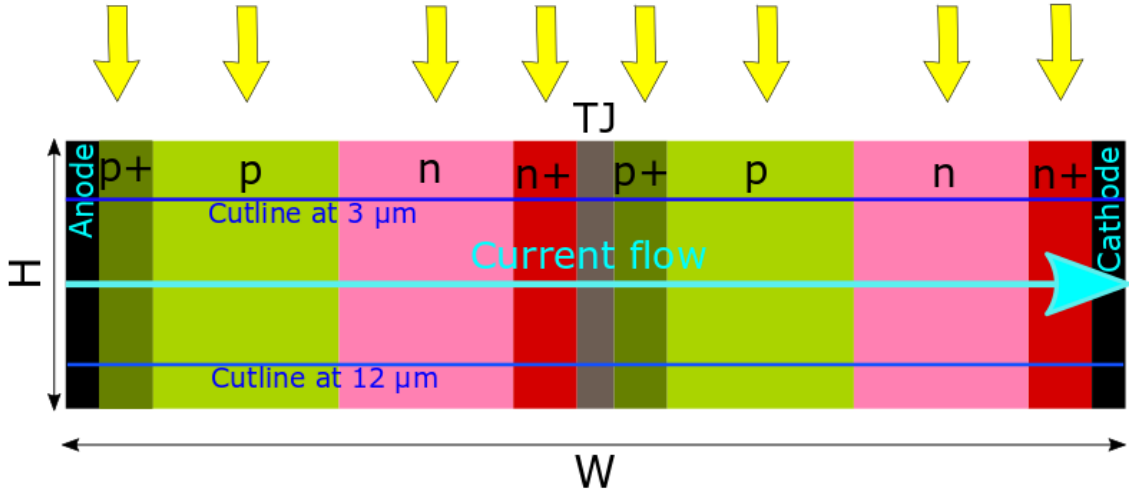

Figure 1: 2D scheme of the VTJ solar cell structure (W: width and H: height).

To obtain the results, Poisson, continuity equations, which relate the electrostatic potential and the carrier densities, were solved using Silvaco Atlas (Silvaco, n.d.). This software is suitable due to its realistic and trustable results for the design and improvement of electronic devices such as multi-bandgap concentrator solar cells (Michael & Bates, 2005).

The optimisation procedure has been carried out considering Concentrator Standard Test Conditions (CSTC), i.e. 1000 W/m^2, AM1.5D reference spectrum, and a 25 ºC (298 K) cell temperature (IEC62670-1:2013, 2013). The structure is illuminated perpendicularly to the PN junctions. The contacts are considered ideal, and we do not account for reflections because the incoming light is parallel to the contacts. The former approximation can be justified considering the low resistance of the contacts, typically ranging from around 10^{-5} to 10^{-7} $\Omega \cdot cm^2$ (Braun, et al., 2012), and the low current flow of the device due to its vertical configuration. All the simulations are done in 2D because we assume that the changes in the third dimension are negligible. Note that heat effects are also not considered at this stage. This is due to the fact that the main intention of this work is to investigate the performance of the new device as a function of C_{ratio}. In any case, future studies will be focused on the thermal behaviour of the novel structure. As previously commented, the solar cell has been optimised for a C_{ratio} of 4000 suns. However, the C_{ratio} has been varied from 1 to 10000 suns in order to evaluate the device in a wide operating condition range.

It is worth mentioning that, at this stage, a VTJ cell only made up of GaAs, including the TJs, has been considered. This avoids any problem of mismatching in the structure and reduces the complexity of the fabrication process, i.e. the structure is lattice-matched and could be monolithically grown. The intention is to propose an architecture as simple as possible to facilitate future work concerning its manufacturing. In addition, this is key to reduce the interface recombination effects among the different layers since the cell is made up of the same material. In any case, future work should also investigate additional layers such as anti-reflective coatings (ARC) or thin Al layers between the PN junctions, which have already shown promising results in Si-based VMJ cells (Tyukhov, 1996). In addition, despite the manufacturing is out of the scope of this paper, further comments regarding its feasibility are also given. The manufacturing of the new device seems possible considering the high accuracy of the growth techniques used in conventional MJ solar cells nowadays, the small cell areas needed, and the electronic devices recently developed based on the multiple connection of around 20 PN junctions by using TJs

(York, et al., 2018). Moreover, the lateral metallic contacts could also be placed on the structure using the same methodology than in current MJ cells. This can be explained considering that the total width of the final VTJ cell, ≈ 0.5 mm, and the height of current MJ cells is similar, ≈ 0.2 mm (Theristis & O'Donovan, 2015).

3. Recombination models

In this work, we studied the main recombination effects, namely: Auger (R_{Auger}), Shockley–Read–Hall (SRH) (R_{SRH}) and optical generation/radiative (R_{rad}). These different effects and the total recombination (R_{total}) are related by the following equation:

$$R_{total}=R_{Auger}+R_{SRH}+R_{rad}\,. \quad (1)$$

If we consider that $R=\frac{1}{\tau}$, the equation (1) can be expressed as (2) in terms of the lifetime (τ), obtaining a total effective lifetime (τ_{eff}) as follows:

$$\frac{1}{\tau_{eff}}=\frac{1}{\tau_{Auger}}+\frac{1}{\tau_{SRH}}+\frac{1}{\tau_{rad}}\,. \quad (2)$$

A brief description of the recombination effects considered in this work is given in the next sub-sections. This is intended to facilitate the understanding of the results of the present investigation.

3.1. Auger

In this recombination process, an electron and hole recombine but a photon is not emitted. The energy is given to another electron, which is excited to a higher energy level. Then, this electron returns to the conduction band due to thermal losses (Selberherr, 1984). This model is important at high current densities and high carrier concentrations such as the produced at UH levels. The standard Auger recombination is modelled by the following expression (Dziewor & Schmid, 1977):

$$R_{Auger}=AUG_n\left(pn^2-nn_{ie}^2\right)+AUG_p\left(np^2-pn_{ie}^2\right), \quad (3)$$

where n and p are the electron and hole concentration respectively, n_{ie}^2 the intrinsic concentration, and AUG_n and AUG_p are, respectively, the Auger coefficients for electrons and holes.

3.2. Shockley-Read–Hall

In SRH, a carrier that is in transition between the bands is trapped by an energy state created by a defect or by a dopant, called trap. Then the energy is exchanged by phonons. This process is dominant in indirect bandgap materials, but it can also dominate in direct bandgap semiconductors if there are many traps. In our simulations, we used the SRH concentration dependent lifetime model because τ also depends on the impurity concentration (Roulston, et al., 1982), (Law, et al., 1991), (Fossum & Lee, 1982). Based on this, the SRH recombination is modelled by the following equation, (Hall, n.d.):

$$R_{SRH}=\frac{pn-n_{ie}^2}{\tau_p\left[n+n_{ie}\exp\left(\frac{E_{trap}}{kT_L}\right)\right]+\tau_n\left[p+n_{ie}\exp\left(\frac{-E_{trap}}{kT_L}\right)\right]}, \quad (4)$$

being

$$\tau_n = \frac{\tau_{n0}}{1+\left(\frac{N_{total}}{N_{SRH_n}}\right)}, \quad (5)$$

$$\tau_p = \frac{\tau_{p0}}{1+\left(\frac{N_{total}}{N_{SRH_p}}\right)}, \quad (6)$$

where E_{trap} is the difference between the trap energy level and the intrinsic Fermi level, T_L the lattice temperature (in Kelvin), k the Boltzmann constant, τ_{n0} and τ_{p0} the electron and hole lifetimes, respectively, N_{total} the total impurity concentration, and N_{SRH_n} and N_{SRH_p} specify the SRH concentration parameter for electrons and holes, respectively.

3.3. Optical generation/Radiative recombination

In this mechanism, the photon transition has to be considered for generation/recombination processes. It is a direct mechanism because occurs in one step. In the radiative recombination, an electron loses energy and moves from the conduction to the valence band emitting a photon with an energy similar to the gap. In the optical generation, an electron moves from the valence to the conduction band. The radiative recombination is the dominant recombination mechanism in direct gap materials, like GaAs, and in narrow gap semiconductors. However, in indirect gap materials this process is very low and then negligible. This model is also called band to band recombination and can be described by equation (7), which means that the total band to band generation/recombination is the difference of the capture rate and emission rate processes:

$$R_{np}^{OPT} = C_C^{OPT}\left(np - n_{ie}^2\right), \quad (7)$$

where C_C^{OPT} means the capture rate.

The parameters considered to take into account the mechanisms above are listed in Table 1.

n_{ie}	$2.67 \cdot 10^6$ cm^{-3} (Grundman, n.d.) , (Vurgaftman, et al., 2001)
AUG_n	$5 \cdot 10^{-30}$ cm^6/s (Picozzi, et al., 2002)
AUG_p	$1 \cdot 10^{-31}$ cm^6/s (Govoni, et al., 2011)
E_{trap}	0 eV (Silvaco, n.d.)
τ_{n0}	$4.4 \cdot 10^{-4}$ s (Lush, et al., 1992)
τ_{p0}	$2.2 \cdot 10^{-4}$ s (Schubert, 2006)
$N_{SRH_{n,p}}$	$2.7 \cdot 10^{13}$ cm^{-3} (Silvaco, n.d.)
C_C^{OPT}	$1.5 \cdot 10^{-10}$ cm^3/s (Olson, et al., 1989)

Table 1: Recombination parameters used in the numerical simulations.

4. Optimisation procedure at 4000 suns concentration

In this section the optimisation of the structure shown in Fig. 1 for a C_{ratio} of 4000 suns is presented. First, the optimisation of the height, by changing its value to maximize the η, was carried out. At this stage, the width and doping values of each layer of our previous

work were considered. An optimum height value of 15 µm was found. Once the height is selected, the width and doping of the n and p layers have been analysed. First, these values were varied for the p-layer while the n-layer parameters were kept constant at 2.5 µm and $1{\cdot}10^{15}$ cm^{-3}. Finally, the n-layer parameters were also optimised by following the same procedure. In this case, the p-layer parameters were kept constant at 5 µm and $1{\cdot}10^{15}$ cm^{-3}. The initial values of each layer to perform the optimisation have been selected based on the structure of the VTJ presented in our previous work.

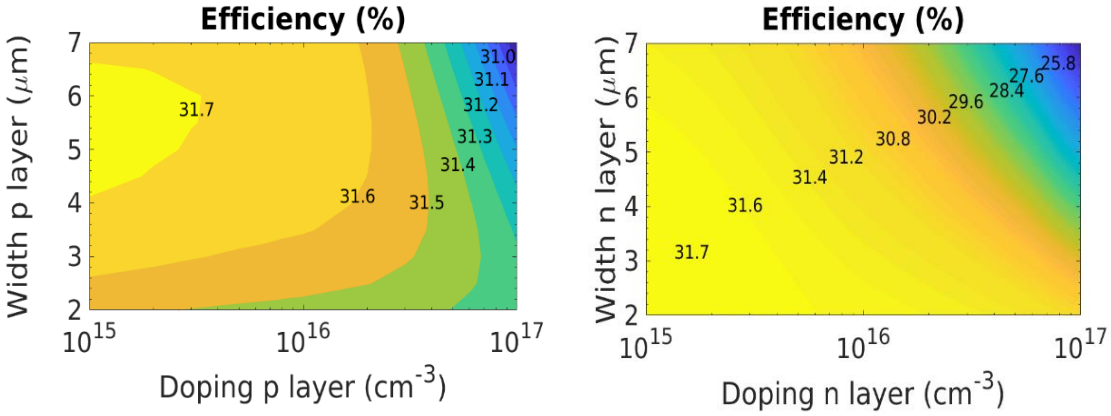

Figure 2: Contour plot of the efficiency as a function of the width and doping of the p-layer (left) and n-layer (right) of the VTJ optimisation at 4000 suns.

Fig. 2 shows the η dependence with the doping and the width for the two layers optimised. As can be seen, for the p-layer (Fig. 2 (left)), η increases as the doping decreases. A maximum η of 31.7 % has been found. This value corresponds to a width ranging from 4.2 to 6.6 µm, and a doping ranging from $1{\cdot}10^{15}$ to $3{\cdot}10^{15}$ cm^{-3}. On the other hand, for the n-layer (Fig. 2 (right)), η also increases as the doping decreases. A maximum η of 31.7 % was obtained for width values between 2.0 and 4.0 µm, and doping values between $1{\cdot}10^{15}$ and $2{\cdot}10^{15}$ cm^{-3}. Based on this study, the width of the p-layer has been considered equal to 6.0 µm, and 3.0 µm for the n-layer. In addition, a doping of $1{\cdot}10^{15}$ cm^{-3} has been considered for both layers. With this configuration, the maximum η, i.e. 31.7 %, for the highest width has been achieved. The latter is crucial to maximize the area of the cell, and therefore to decrease the number of TJs as much as possible for structures based on the tunnelling connection of multiple VTJ cells.

As can be also seen in Fig. 2, η is more sensitive to the width and doping variations in the n-layer (η varies from 25.8 % to 31.7 %) than in the p-layer (η varies less than 1 %). This can be understood considering the different electron and hole mobilities (µ) for the layers and their relation with the L, i.e. the higher the µ the higher the L (Markvart & Castañer, 2005). In the p-layer, Fig. 2 (left), the n minority carriers have a higher µ, which implies a better carrier collection in the electrodes. As a consequence, the short-circuit current (I_{SC}), and therefore η, are less sensitive to the width and doping variations. This can be understood considering that η is proportional to I_{SC}:

$$\eta = \frac{I_{SC}\, V_{OC} FF}{P_{in}} = \frac{P_{max}}{P_{in}} \quad , \qquad (8)$$

where V_{OC} the open-circuit voltage, FF the Fill Factor, and P_{in} and P_{max} are the incident and maximum power output, respectively. On the other hand, in the n-layer, Fig. 2 (right), the p minority carriers have a lower µ. Hence, the carrier collection in the electrodes is

lower than in the previous case. As a consequence, the I_{SC}, so the η, are more sensitive under the width and doping variations.

In addition to the effects above, the different carrier concentration between the two layers also contributes to enhance their different behaviour under width and doping variations. The n-layer has more carriers, so, the recombination effects in this layer become more relevant, being the radiative and SRH recombination mechanisms the most affected (see section 5). These rates increase with the number of carriers, as can be obtained from the analysis of the equations (4) and (7), and therefore the τ_{eff} tends to decrease. As in the previous case, this contributes to reduce L, and therefore η is more affected under the width and doping variations in this layer.

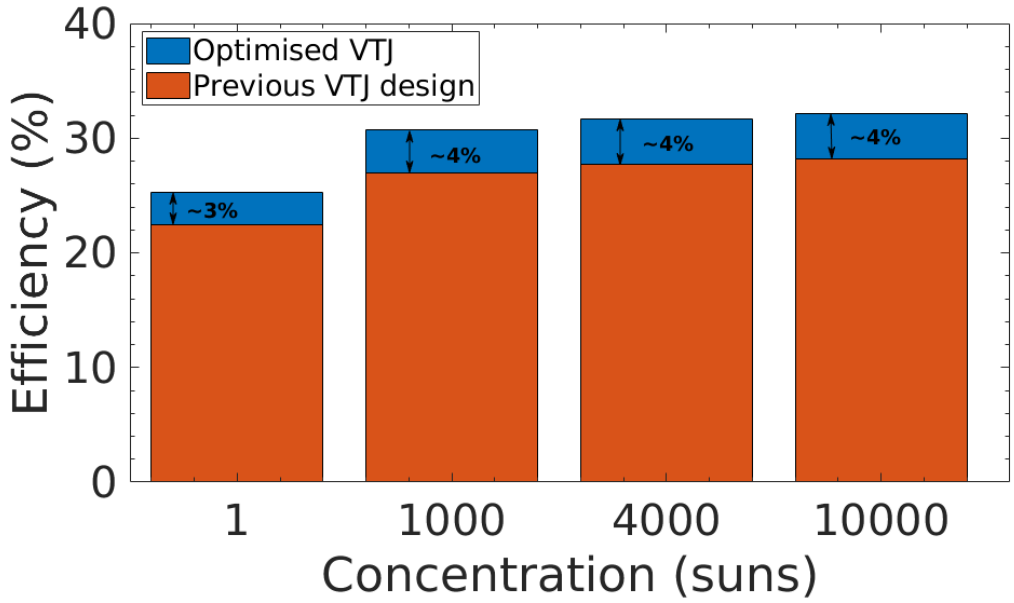

Figure 3: Comparison of the efficiency between the VTJ of this work (Fig. 1) and the structure of our previous work (Fernández, et al., 2019).

Fig. 3 shows a comparison of the η between the optimised structure of this work and the results of our previous design for C_{ratio} ranging from 1 to 10000 suns. As can be seen, the optimised design strongly improves the η. These η values are around 4 % higher than in the previous design except for C_{ratio} of 1 sun, which is around 3 % higher. The optimisation procedure conducted in this section allows solar cells with record η above 30 % at ultra-high concentration factors to be developed.

5. Numerical results

In this section, first, the effect of the different recombination mechanisms and their total effect on the V_{OC}, I_{SC} and P_{max} at 4000 suns have been studied. After that, the main recombination mechanisms and their impact on the key electrical parameters as a function of C_{ratio} have been investigated.

5.1. Impact of recombination

First, the effect of the Auger, radiative, SRH and their combined total recombination in the V_{OC} point was analysed, under a C_{ratio} of 4000 suns. The different recombination

effects along the width of the VTJ structure at 3 and 12 µm on the vertical direction from the incident light surface, see Fig. 1, are shown in Fig. 4 (a) and (b), respectively.

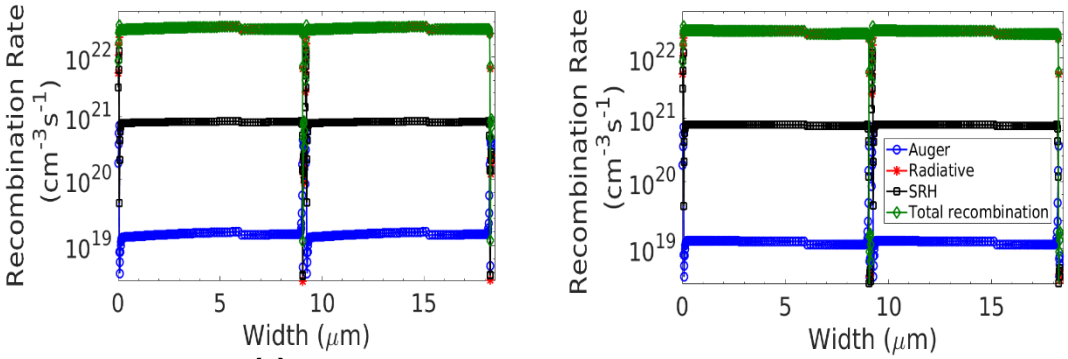

Figure 4: Cutlines along the width of the device structure in 3 (a) and 12 (b) µm, see Fig. 1, under 4000 suns at the V_{OC} point.

To properly compare the recombination rates among the different effects, the middle points of the p and n-layers were selected for each subcell. Those points are located at width values of 3.0 and 12.2 µm for the p-layers, and at 8.0 and 17.2 µm for the n-layers. When the height is 3 µm, the total recombination is $3.2 \cdot 10^{22}$ and $3.0 \cdot 10^{22}$ $cm^{-3}s^{-1}$ for the p and n-layers, respectively. As expected, these values are identical for both the first and second subcells. When the height is 12 µm, the total recombination values decrease to $2.9 \cdot 10^{22}$ and $2.6 \cdot 10^{22}$ $cm^{-3}s^{-1}$ for the p and n-layers, respectively. This can be explained considering that the intensity of the incident flux drops the farther you move from the surface where the light is falling on. The relative difference for the total recombination between the two height values is 9.4 % in the p-layers points, and 13.3 % in the n-layers points. The radiative recombination is the dominant effect, being the 97.3 % of the total recombination (at 3 and 8 µm widths and 3 µm height), and 97.3 % and 97.0 % (at a 3 and 8 µm widths and 12 µm height). This was expected considering that GaAs is a direct bandgap semiconductor. The mechanism with the lower impact is Auger, about three orders of magnitude lower than that of radiative. It represents an almost negligible 0.05 % of the total recombination (at a 3 µm and 8 µm width and 3 µm height), and 0.04 % (at a 3 µm and 8 µm width and 12 µm height). Similar results were previously reported by (Ochoa, et al., 2016) and (Wang, et al., 2013). The SRH recombination contributes with a 2.6 % and 2.7 % to the total recombination (at a 3 µm and 8 µm width and 3 µm height), and 2.7 % and 2.9 % (at a 3 µm and 8 µm width and 12 µm height). SRH is around one order of magnitude lower than the radiative recombination.

At this point, the effect of the Auger, radiative, SRH and their combined total recombination in the I_{SC} point was analysed, under a C_{ratio} of 4000 suns. The different recombination effects along the width of the VTJ structure at 3 and 12 µm on the vertical direction from the incident light surface are shown in Fig. 5 (a) and (b) respectively.

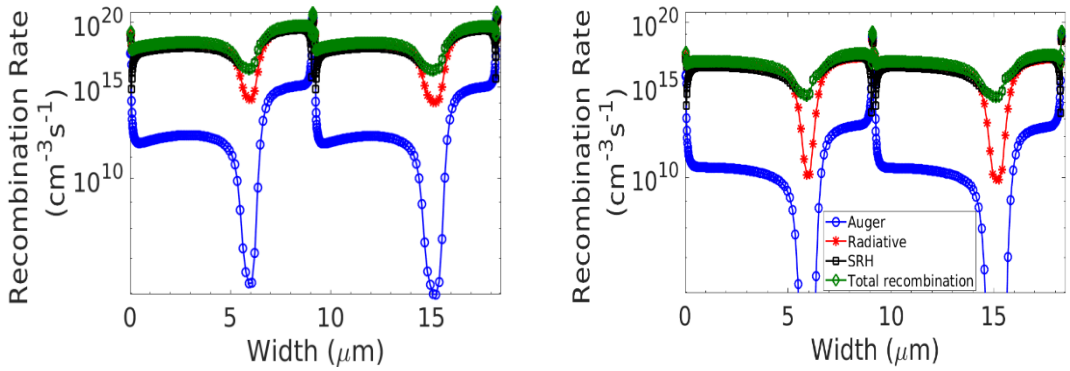

Figure 5: Cutlines along the width of the device structure in 3 (a) and 12 (b) μm, see Fig. 1, under 4000 suns at the I_{SC} point.

Like in the previous case, to properly compare the recombination rates among the different effects, the same middle points of the p and n-layers were selected for each subcell. In this case, the total recombination is $2.1 \cdot 10^{18}$ and $4.8 \cdot 10^{19}$ $cm^{-3}s^{-1}$ for the p and n-layers respectively at 3 μm height. As expected, these values are identical for both the first and second subcells. When the height is 12 μm, the total recombination values decrease to $5.0 \cdot 10^{16}$ and $2.3 \cdot 10^{17}$ $cm^{-3}s^{-1}$ for the p and n-layers, respectively. The relative difference for the total recombination between the two height values is 97.6 % in the p-layers points, and 99.5 % in the n-layers points. Once again, the radiative recombination is the dominant effect, being the 63.8 % and 55.9 % of the total recombination (at a 3 μm and 8 μm width respectively and 3 μm height), and a 63.4 % and 46.5 % (at a 3 μm and 8 μm width respectively and 12 μm height). The effect of Auger can be considered marginal as this only represents a value lower than 0.002 % of the total recombination for the analysed points. The radiative recombination is about six orders of magnitude larger than that of Auger in the p-layers, and four orders in the n-layers. The SRH recombination contributes with a 36.2 % and 44.0 % to the total recombination (at a 3 μm and 8 μm width respectively and 3 μm height), and a 36.6 % and 53.5 % (at a 3 μm and 8 μm width respectively and 12 μm height). As for the case of the V_{OC}, SRH is around one order of magnitude lower than the radiative recombination in the p-layers and the same order in the n-layers.

Finally, the effect of the different recombination mechanisms and their combined total value in the P_{max} point under 4000 suns have been analysed. It is important to note that, at P_{max} less carriers will be recombined than in the V_{OC} point, but more than in the I_{SC}, so, the recombination rates are expected to be smaller than the V_{OC} case but higher than in the I_{SC}.

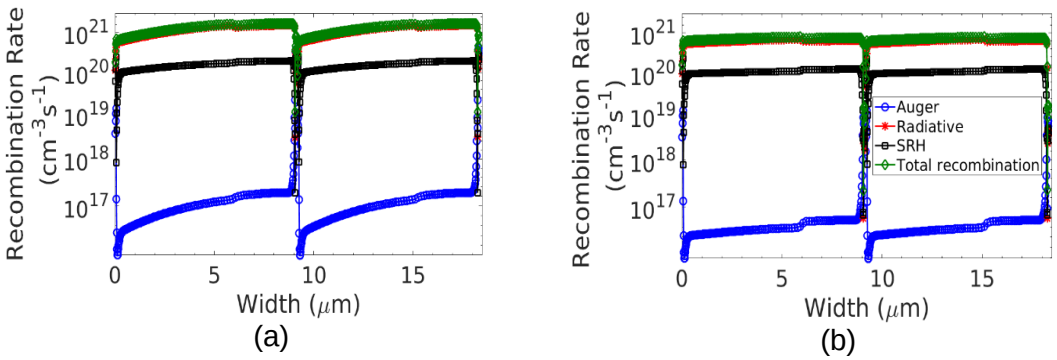

Figure 6: Cutlines along the width of the device structure in 3 (a) and 12 (b) μm, see Fig. 1, under 4000 suns at the P_{max} point.

As in the previous two cases, the different recombination effects along the width of the VTJ structure at 3 and 12 μm from the incident light surface are shown in Fig. 6 (a) and (b) respectively at the P_{max} point. Like in the previous analyses, to properly compare the recombination rates among the different effects, the same middle points for the p and n-layers than above were selected for each subcell. As can be seen in the figure, the total recombination for the cutline in 3 μm is $1.2 \cdot 10^{21}$ and $1.7 \cdot 10^{21}$ $cm^{-3}s^{-1}$ for the p and n-layers, respectively. On the other hand, for the cutline made at 12 μm, the values for the p and n-layers are $7.2 \cdot 10^{20}$ and $7.5 \cdot 10^{20}$ $cm^{-3}s^{-1}$, respectively. The relative difference for the total recombination between the two cutlines is 40 % in the p-layers, and 55.9 % in the n-layers. The radiative recombination is the dominant effect, being the 88.2 % and 88.7 % of the total recombination (at a 3 μm and 8 μm width respectively and 3 μm height), and the 85.4 % and 83.4 % (at a 3 μm and 8 μm width respectively and 12 μm height), because we have a direct bandgap semiconductor.

Like for the V_{OC} and I_{SC} results, the effect of Auger is negligible and represents less than 0.01 % for all the cases analysed. The difference between the radiative and Auger recombination is about four orders of magnitude. The SRH recombination contributes with a 11.8 % and 11.3 % (at a 3 μm and 8 μm width respectively and 3 μm height), and a 14.6 % and 16.6 % (at a 3 μm and 8 μm width respectively and 12 μm height). In this case, SRH is around one order of magnitude lower than the radiative recombination in the 3 μm height cutline and has the same order of magnitude in the 12 μm height cutline for both layers. As expected, all these percentages values are identical for both the first and second layers.

5.2 *Impact of solar concentration on the electrical parameters*

In this section, we study the effect of C_{ratio} on the electrical parameters, i.e. I_{SC}, V_{OC}, FF and η, of the solar cell. In addition, we consider the different recombination mechanisms, i.e. Auger, radiative and SRH, in order to fully understand the performance and possible limitations of the device.

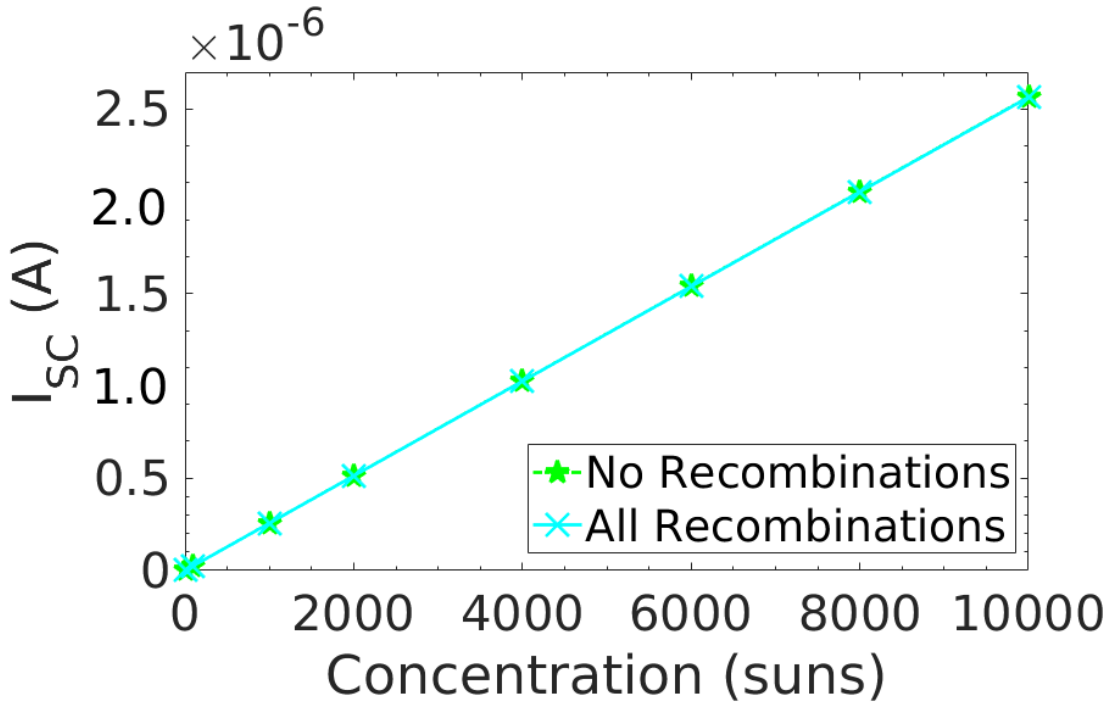

Figure 7: Short-circuit current as a function of C_{ratio} for the VTJ solar cell without considering any recombination effect and with all recombination effects.

Fig. 7 shows the I_{SC} as a function of C_{ratio} for the VTJ solar cell when no recombination effects have been considered and when all effects have been taken into account. As can be seen, this parameter increases linearly with C_{ratio} for both cases, with a determination coefficient (R^2) of 0.99. This suggests that the I_{SC} is not affected by neither of the recombination's mechanisms investigated. It is also important to mention the low current values reached by the cell even for extreme concentration ratios. This is also key to diminish the series resistance limitations of current concentrator solar cells. The maximum current is dominated by the small illumination area of the VTJ cell, which is defined by the width of the PN junctions of the structure. This value, which is around 10 µm, is approximately three order of magnitude lower than in current horizontal MJ cells, which is around 5 mm. Further discussion about this topic can be also found in the early work of the authors (Fernández, et al., 2019).

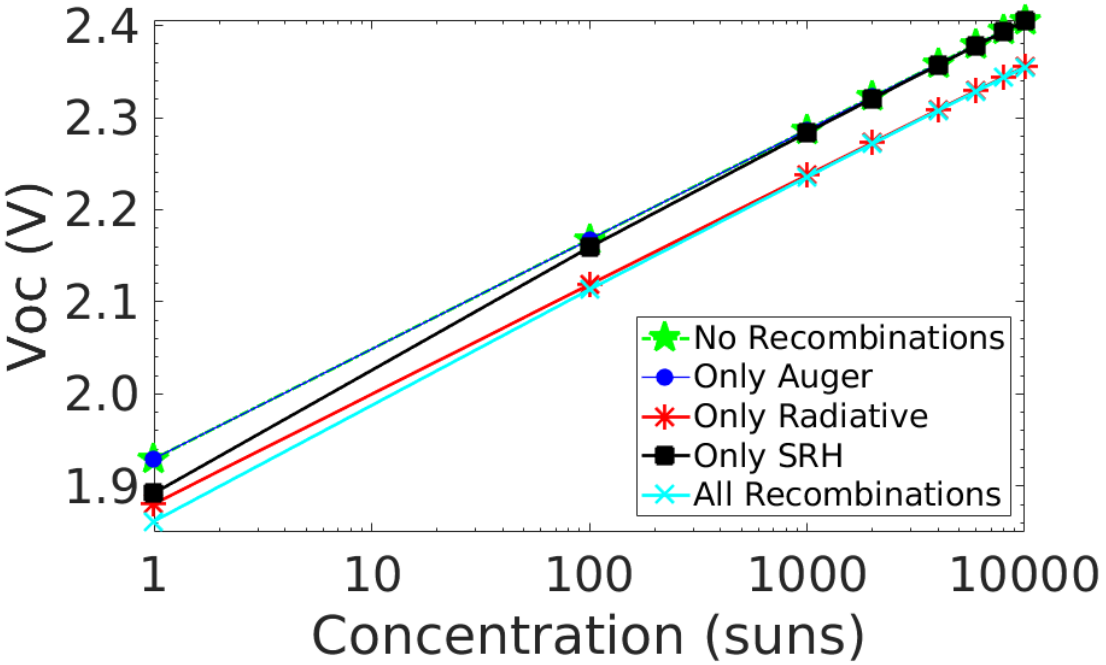

Figure 8: Open-circuit voltage as a function of C_{ratio} for the VTJ solar cell without recombinations, for each recombination mechanism and for all recombinations.

Fig. 8 presents the V_{OC} as a function of the C_{ratio} for the VTJ solar cell, showing both the individual contributions of the three analysed recombination effects (Auger, radiative and SRH) and their combined effect (all recombinations). Note that a scenario without any recombination effect has also been considered for comparison purposes.

The figure shows that V_{OC} grows linearly with the logarithm increase of C_{ratio} for all the recombination mechanisms. It varies from ≈ 1.86 V at 1 sun to ≈ 2.35 V at 10000 suns when all the mechanisms are considered. The presence of all recombination effects lowers the V_{OC} by 3.5 % (for 1 sun) and by 2.1 % (for 10000 suns), with respect to the ideal case. In this figure, it can also be seen that the V_{OC} is affected by the SRH and radiative similarly up to 100 suns. For larger sun concentrations, the radiative is the dominant effect and degrades the V_{OC} the most, whereas the effect of SRH becomes insignificant. This can also be concluded by analysing the ideality factor (m) of the different mechanisms as a function of the C_{ratio} relative to its value at any reference concentration ($C_{ratio,ref}$) (Siefer & Bett, 2014), (Braun, et al., 2013):

$$V_{OC}(C_{ratio}) - V_{OC}(C_{ratio,ref}) \approx \frac{m}{N} V_T \ln\left(\frac{C_{ratio}}{C_{ratio,ref}}\right), \quad (9)$$

where N is the number of PN junctions in series (two in this case) and V_T is the thermal voltage. For $C_{ratio} \leq 100$ suns the m obtained when considering all the recombinations is 1.06, while for higher C_{ratio} become equal to 1.00. On the other hand, the m for the SRH case is 1.12 ($C_{ratio} \leq 100$ suns) and 1.04 ($C_{ratio} > 100$ suns), while it becomes almost independent of the C_{ratio} for the radiative case, with a value of m = 1.00. The aforementioned variations of m are certainly small, but they also seem to suggest that SRH has a more significant effect on the recombination mechanisms at lower C_{ratio}, while the performance of the cell is dominated by radiative mechanisms at higher C_{ratio}.

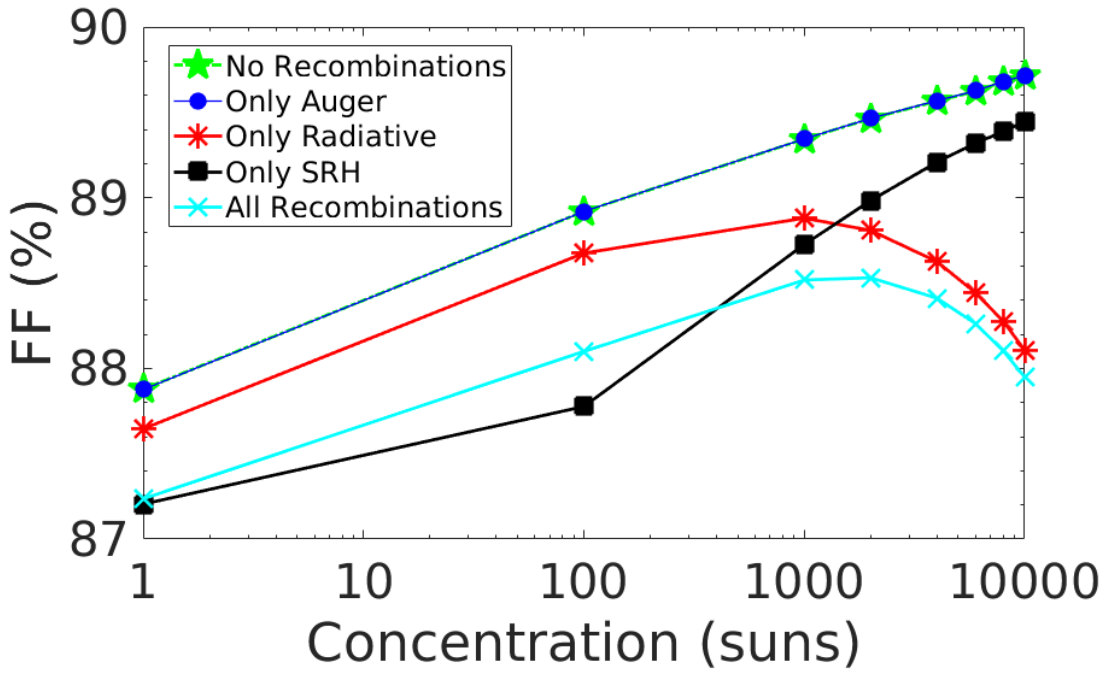

Figure 9: Fill Factor as a function of C_{ratio} for the VTJ solar cell without recombinations, for each recombination mechanism and for all recombinations.

Fig. 9 presents the FF as a function of C_{ratio} for the VTJ solar cell, showing both the individual contributions of the three analysed recombination effects (Auger, radiative and SRH) and their combined effects (all recombinations). For this scenario it was also considered the case where no recombination effects were included for comparison purposes.

As can be seen in the figure, the FF increases with the logarithm increase of the C_{ratio} for the no recombination effects, Auger and SRH cases. Nevertheless, for the radiative and all recombination cases, FF grows with the C_{ratio} up to 1000 and 2000 suns respectively, whereas for higher irradiances the FF tends to decrease. It varies from ≈ 87.23 % at 1 sun to 88.53 % at 2000 suns when all the mechanisms are considered. Above this C_{ratio}, the FF slightly decreases due to R_S losses up to a value of 87.95 % at 10000 suns. Despite this, FF shows a small range of variation for all the C_{ratio} investigated (≈ 1 %). This is a crucial finding since the FF of current MJ cells usually decreases around 5 % for a much more lower C_{ratio} range, i.e. usually from 500 to 1000 suns (Kinsey, et al., 2008), and this is in fact the main limiting factor of current devices to achieve high efficiencies at UH levels. This slight variation is due to the small R_S values of the VTJ solar cell. Indeed, the R_S value has been estimated from the simulated IV curve at 4000 suns using the methods previously discussed by the authors in (Fernández, et al., 2016), and a value ≈ 1.5 10^{-3} Ω·cm^2 has been found, around one or two orders of magnitude lower than that of conventional concentrator solar cells (Appelbaum & Peled, 2014).

Regarding the different recombination mechanisms, at C_{ratio} below 1000 suns, the SRH recombination is dominant and contributes to the FF the most. For C_{ratio} > 2000 suns, the effect of SRH decreases and radiative becomes the dominant source of degradation of the FF. Also, compared to the ideal case, the degradation of FF is larger at UH irradiances (1.8 % at 10000 suns) than at low irradiances (0.6 % at 1 sun). This is due to the fact that the SRH recombination plays an important role for C_{ratio} up to 1000 suns.

It is important to note that FF is lower for the SRH case with respect to the all recombinations one up to 100 suns. In order to understand this behaviour, Figs. 10 and

11 present the IV curves, and key electrical parameters, for three different recombination scenarios (only radiative, only SRH and all recombinations) at 100 suns and 4000 suns, respectively. For a C_{ratio} of 100 suns the V_{OC} for the SRH case is around 2.4 % higher than that of all recombinations. However, the P_{max} of the SRH recombination only grows by 1.9 %. As consequence the FF decreases in a larger extend since this is given by:

$$FF = \frac{P_{max}}{I_{SC} \cdot V_{OC}} . \qquad (10)$$

On the other hand, for a C_{ratio} of 4000 suns, the V_{OC} for the SRH case is also higher, around 2.2 %, than that of all recombinations. However, in this case, the P_{max} grows around 3.3 %. As consequence, the FF becomes higher than the value when all the effects are considered.

The phenomenon above could be explained by analysing the saturation current (I_0) for the different cases. This value has been extracted by using the Phang model (Phang, et al., 1984), also previously validated to investigate concentrator solar cells by the authors (Fernández, et al., 2016). At 100 suns, the SRH is the main contributor to the all recombinations and presents a I_0 value three orders of magnitude larger, I_0 =1.50 10^{-19} A, with regards to the only radiative, I_0 = 6.75 10^{-22} A. This high value of I_0 degrades the IV curve in a larger extend and could explain the smaller increase of the P_{max} respect to the V_{OC}. It is also important to mention that the higher V_{OC} values of the SRH case are due to a higher m value previously estimated, m (radiative) = 1.00 while m (SRH) = 1.12. However, at a higher C_{ratio} of 4000 suns, radiative is the main recombination effect, the I_0 is around eight times larger, I_0 = 8.38 10^{-20} A, with respect to the only SRH, which is 1.14 10^{-20} A. In addition, the I_0 for the SRH case is lower than that at 100 suns. As a consequence, the IV is less affected and could also explain why P_{max} grows in larger extent than V_{OC}, and therefore, why the FF is higher at UH C_{ratio} with respect to the all recombination case.

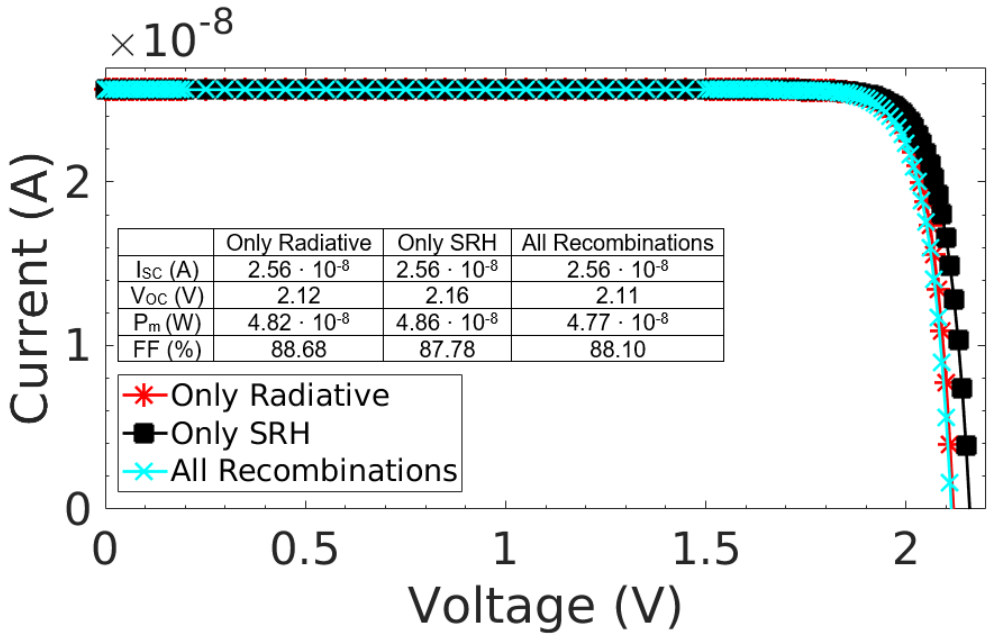

	Only Radiative	Only SRH	All Recombinations
I_{SC} (A)	$2.56 \cdot 10^{-8}$	$2.56 \cdot 10^{-8}$	$2.56 \cdot 10^{-8}$
V_{OC} (V)	2.12	2.16	2.11
P_m (W)	$4.82 \cdot 10^{-8}$	$4.86 \cdot 10^{-8}$	$4.77 \cdot 10^{-8}$
FF (%)	88.68	87.78	88.10

Figure 10: I-V curves and some electrical parameters for the only radiative, only SRH and all recombinations case with a C_{ratio} of 100 suns.

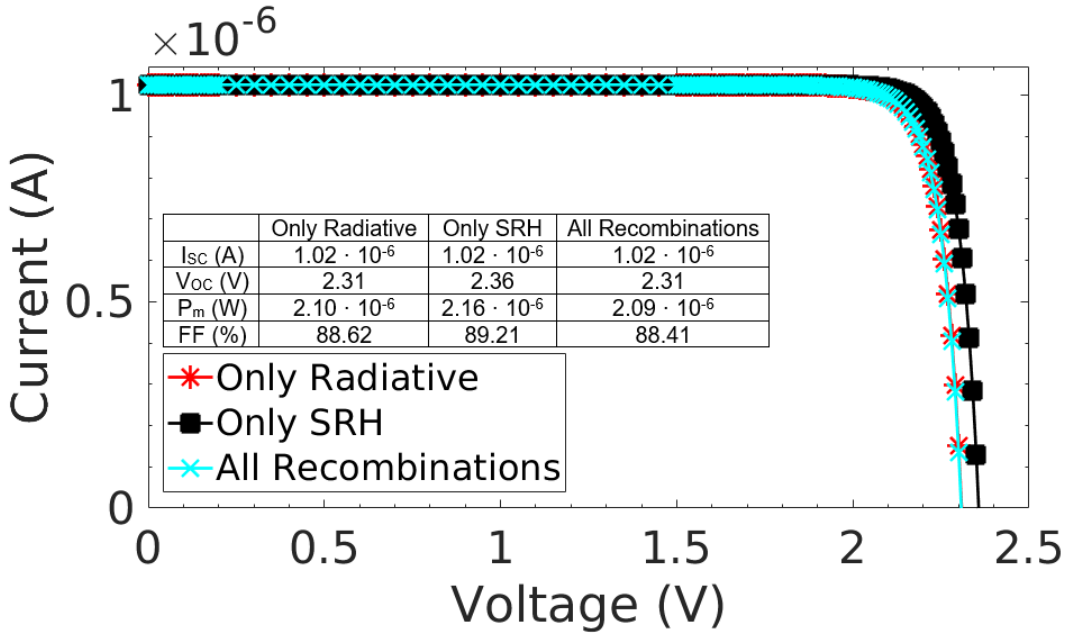

	Only Radiative	Only SRH	All Recombinations
I_{SC} (A)	$1.02 \cdot 10^{-6}$	$1.02 \cdot 10^{-6}$	$1.02 \cdot 10^{-6}$
V_{OC} (V)	2.31	2.36	2.31
P_m (W)	$2.10 \cdot 10^{-6}$	$2.16 \cdot 10^{-6}$	$2.09 \cdot 10^{-6}$
FF (%)	88.62	89.21	88.41

Figure 11: I-V curves and some electrical parameters for the only radiative, only SRH and all recombinations case with a C_{ratio} of 4000 suns.

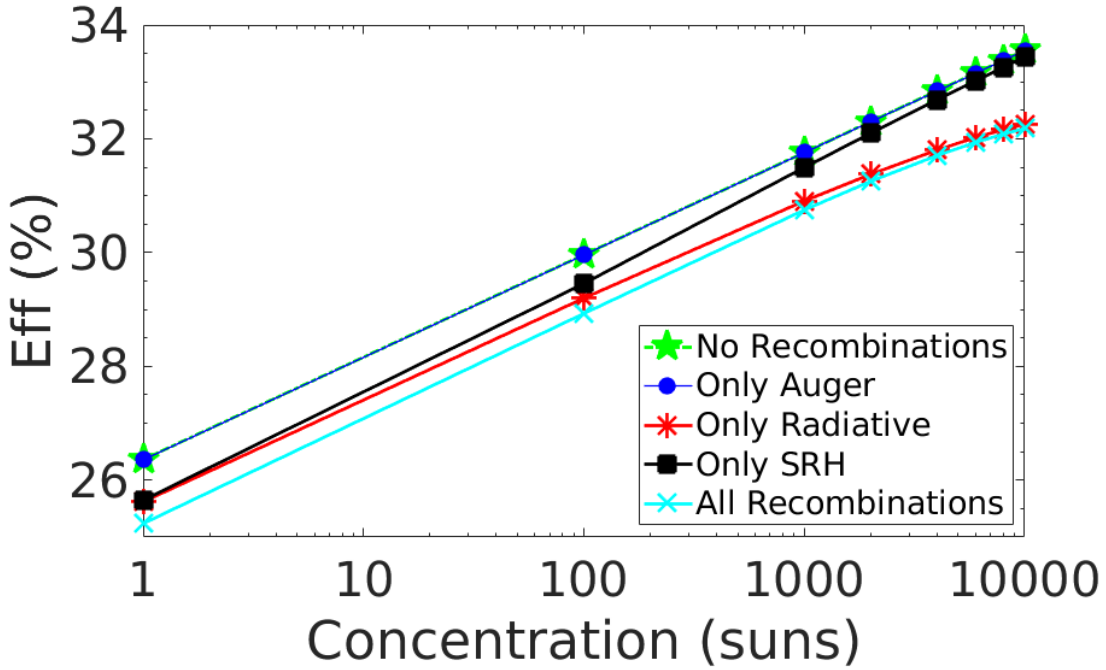

Figure 12: Efficiency as a function of C_{ratio} for the VTJ solar cell without recombinations, for each recombination and for all recombinations.

Fig. 12 presents the η as a function of the C_{ratio} for the VTJ solar cell, showing both the individual contributions of the three analysed recombination effects (Auger, radiative and SRH), and their combined effects (all recombinations). As previously, it was also considered the no recombinations case for comparison. It is also important to mention that Auger effects are negligible even at extreme C_{ratio} of 10000 suns. This is relevant considering that this mechanism has been previously signalled by other researchers as the ultimate limiting factor to produce device valid to achieve UH levels due to the large amount of carriers generated (Govoni, et al., 2011).

As shown in the figure, η increases almost linearly with the logarithm increase of C_{ratio} for all the cases. The small reduction of the FF previously signalled for C_{ratio} above 2000 suns does not limit the performance of the device with C_{ratio}. η varies from ≈ 25.2 % at 1 sun to a maximum value of ≈ 32.2 % at 10000 suns. Regarding the recombination mechanisms, at low C_{ratio} below 100 suns, the SRH and radiative recombinations contribute similarly to the reduction in the η. For larger C_{ratio}, the radiative is the dominant effect and degrades the η the most. At the same time, the SRH effect becomes insignificant as the C_{ratio} increases. It was also found that the reduction of η due to all recombination contributions is higher at UH irradiances (1.4 % at 10000 suns) than at low irradiances (1.1 % at 1 sun). This is due to the fact that the radiative mechanism dominates as the C_{ratio} is increased. Hence, the small reduction in the FF introduced by this mechanism with the C_{ratio}, see Fig. 9, also contributes to degrade the η to a greater amount, see also equation (8).

Despite of the above, the η achieved by the optimised VTJ cell would represent a record η solar cell, which is nowadays 29.3 % for a GaAs conventional structure at a C_{ratio} ≈ 50 suns (Green, et al., 2018), far below the solar concentration levels here investigated. This represents a promising route to deliver single-band-gap structures with state-of-the-art η > 30 % due to the elimination of the series resistance constraints.

6. Conclusions

In this work, we have studied a novel structure based on gallium arsenide (GaAs) previously proposed by the authors in a short communication. This structure was optimised at a concentration ratio (C_{ratio}) of 4000 suns in order to improve the device efficiency (η). Once the device was optimised, the effect of the different recombination mechanisms and their total effect on the open-circuit voltage (V_{OC}), short-circuit current (I_{SC}) and the maximum power (P_{max}) was studied along the width of the vertical-tunnel-junction (VTJ) structure. Finally, the impact of the main recombination mechanisms on the key electrical parameters as a function of C_{ratio} was investigated.

For this structure, it was carried out an optimisation of the device height and the width and doping of the p and n layers. As a result of this procedure, a maximum η value of 31.7 % for a C_{ratio} of 4000 suns was demonstrated. This significantly improves the η of our previous design by a value ranging from 3 % to 4 % for all the C_{ratio} analysed.

For this solar cell, the radiative recombination is the dominant mechanism. For the V_{OC}, this mechanism is around 97.3 % of the total recombination. For the $P_{max,}$ it is around the 88.0 % (at a 3 μm cutline along the width of the VTJ structure). Nevertheless, at the I_{SC} point, the radiative recombination is 63.8 % and 55.9 % of the total recombination for the p and n-layers respectively, whereas the SRH recombination is 36.2 % (p-layers) and 44.0 % (n-layers) of the total recombination (at a 3 μm cutline). These recombination rates decreased as we moved away from the surface where the light was falling on. It was found Auger recombination was almost negligible for all the parameters.

In addition, our study indicated that the behaviour of the key electrical parameters was not limited by neither of the recombination mechanisms. The I_{SC} grew linearly with the C_{ratio} independently of the recombination mechanism considered and it is not affected by neither of them. The V_{OC} also increased linearly with the logarithm of the C_{ratio}. It was found that the all recombination effects lowered this magnitude less at extreme concentrations (2.1 % at 10000 suns) than a low C_{ratio} (3.5 % at 1 sun) with respect to the ideal case. Results also showed that at C_{ratio} above 100 suns the dominant mechanism was radiative recombination, whereas at low C_{ratio} the radiative and SRH

contributions were similar. For the Fill Factor (FF), it was found that for all recombination case it grew up to 2000 suns and then decreased with the logarithm of C_{ratio}. The maximum FF value obtained was 88.53 % at 2000 suns. Above this C_{ratio}, the FF slightly decreased, obtaining a value of 87.95 % for 10000 suns.

Results showed a linear increase in the η of the VTJ solar cell with C_{ratio} and no remarkable impact (maximum observed η degradation of 1.37 % at 10000 suns respect the ideal case) caused by the recombination mechanism investigated. For C_{ratio}<100 suns the SRH and radiative recombinations contributed similarly to the η reduction, whereas for C_{ratio}>100 suns the radiative recombination dominated and degraded the η the most. A maximum η of 32.2 % at 10000 suns was obtained. This would represent a record η, being currently a 29.3 % for GaAs conventional structures at a C_{ratio} of 50 suns, at C_{ratio} far above any previous solar cell found in the literature. This highlights the interest and potential of the vertical solar cell here investigated to produce a new type of structure tailored to achieve extreme C_{ratio}.

Future work should investigate the performance of the cell under temperature, spectrum and uniformity variations. In addition, structures made up of different materials and/or with additional layers, such as anti-reflective coatings (ARC), should be considered in order to enhance the potential efficiency of the device. Finally, the investigation of multi-band-gap structures made up of several VTJs aimed to optimise the absorption of the spectrum should be the topic of further investigations. This could be achieved by mechanically stacking multiple VTJ solar cells made up of different materials and energy gaps on the top of each other in decreasing order of the band-gap.

Acknowledgement

E. F. Fernández and F. Almonacid thank the Spanish Economy Ministry and FEDER funds received under the project ENE2016-78251-R. N. Seoane and A. J. García Loureiro thank Spanish Ministry of Economy and Competitiveness and FEDER funds (TIN2016-76373-P) and the Xunta de Galicia and FEDER funds (GRC 2014/008). N. Seoane and E.F. Fernández also thank the Spanish Ministry of Science, Innovation and Universities (RYC-2017-23312, RYC-2017-21910). C. Outes also thanks the Ayudas predoctorales para la Formación de Personal Investigador con cargo a la Acción 9.a) del Plan de Apoyo a la Investigación de la Universidad de Jaén (ERC_2019_1).

References

Algora, C. & Rey-Stolle, I., 2012. The Interest and Potential of Ultra-High Concentration. In: *Next Generation of Photovoltaics.* s.l.:Springer, pp. 23-60.

Appelbaum, J. & Peled, A., 2014. Parameters extraction of solar cells - A comparative examination of three methods. *Solar Energy Materials and Solar Cells,* Volume 122, pp. 164-173.

Barrigón, E. et al., 2014. Highly conductive p + +-AlGaAs/n + +-GaInP tunnel junctions for ultra-high concentrator solar cells. *Progress in Photovoltaics: Research and Applications,* 22(4), pp. 399-404.

Braun, A. et al., 2013. Temperature dynamics of multijunction concentrator solar cells up to ultra-high irradiance. 21(2), pp. 202-208.

Braun, A. et al., 2012. Multi-bandgap vertical-junction architectures for ultra-high-efficient concentrator cells. *Energy & Environmental Science,* Volume 5, pp. 8523-8527.

Cotal, H. et al., 2009. III-V multijunction solar cells for concentrating photovoltaics. *Energy and Environmental Science,* 2(2), pp. 174-192.

Dziewor, J. & Schmid, W., 1977. Auger coefficients for highly doped and highly excited silicon.. *Applied Physics Letters,* Issue 31, pp. 346-348.

Fernández, E. F. et al., 2016. Comparative study of methods for the extraction of concentrator photovoltaic module parameters.. *Solar Energy,* Volume 137, pp. 413-423.

Fernández, E. F., Talavera, D. L., Almonacid, F. & Smestad, G. P., 2016. Investigating the impact of weather variables on the energy yield and cost of energy of grid-connected solar concentrator systems. *Energy,* Volume 106, pp. 790-801.

Fernández, E., Seoane, N., Almonacid, F. & García-Loureiro, A., 2019. Vertical-tunnel-junction (vtj) solar cell for ultra-high light concentrations (>2000 suns).. *IEEE Electron Device Letters,* Issue 40, pp. 40-47.

Ferrer-Rodríguez, J., Fernández, E., Almonacid, F. & Pérez-Higueras, P., 2016. Optical design of a 4-off-axis-unit Cassegrain ultra-high concentrator photovoltaics module with a central receiver. *Optics Letters ,* 41(9), pp. 1985-1988.

Ferrer-Rodriguez, J. P. et al., 2020. Exploring ultra-high concentrator photovoltaic Cassegrain-Koehler-based designs up to 6000×. *Optics Express,* Volume In press.

Fossum, J. G. & Lee, D. S., 1982. A physical model for the dependence of carrier lifetime on doping density in nondegenerate silicon.. *Solid-State Electronics,* Issue 25, pp. 741-747.

García, I., Rey-Stolle, I. & Algora, C., 2012. Performance analysis of AlGaAs/GaAs tunnel junctions for ultra-high concentration photovoltaics. *Journal of Physics D: Applied Physics,* 45(4), p. 045101.

Gover, A. & Stella, P., 1974. Vertical multijunction soalr-cell one-dimensional analysis. *IEEE Transactions on Electron Devices,* pp. 351-356.

Govoni, M., Marri, I. & Ossicini, S., 2011. Auger recombination in Si and GaAs semiconductors: Ab initio results.. *Physical Review B,* August, Volume 84, p. 075215.

Green, M., 2020. Solar cell efficiency tables (version 55). *Progress in Photovoltaics: Research and Applications,* 28(1), pp. 3-15.

Green, M. A. et al., 2018. Solar cell efficiency tables (version 52). *Progress in Photovoltaics: Research and Applications,* 26(7), pp. 427-436.

Grundman, M., n.d. *The Physics of Semiconductors. An Introduction Including Nanophysics and Applications..* Third Edition ed. s.l.:Springer.

Hall, R., n.d. Electron-hole recombination in germanium.. *Phys. Rev.,* Issue 87, pp. 387-387.

IEC62670-1:2013, 2013. *Photovoltaic concentrators (CPV)-Performance testitng- Part1: Standard conditions,* s.l.: s.n.

Kamath, H., Ekins-Daukes, N., Araki, K. & Ramasesha, S., 2019. The potential for concentrator photovoltaics: A feasibility study in India. *Progress in Photovoltaics: Research and Applications,* 27(4), pp. 316-327.

Kinsey, G. S. et al., 2008. Concentrator Multijunction Solar Cell Characteristics Under Variable Intensity and Temperature. *Progress in Photovoltaics: Research and Applications,* 16(6), pp. 503-508.

Law, M. E., Solley, E., Liang, M. & Burk, D. E., 1991. Self-consistent model of minority-carrier lifetime, diffusion length, and mobility.. *IEEE Electron Device Letters,* Issue 12, pp. 401-403.

Lush, G. B. et al., 1992. A study of minority carrier lifetime versus doping concentration in n-type GaAs grown by metalorganic chemical vapor deposition. *Journal of Applied Physics,* 72(4), pp. 1436-1442.

Markvart, T. & Castañer, L., 2005. *Solar Cells. Materials, manufacture and operation.* First ed. s.l.:Elsevier.

Michael, S. & Bates, A., 2005. The design and optimization of advanced multijunction solar cells using the silvaco atlas software package.. *Solar Energy Materials and Solar Cells,* Volume 87, pp. 785-794.

Ochoa, M. et al., 2016. Limiting factors on the semiconductor structure of III–V multijunction solar cells for ultra-high concentration (1000–5000 suns). *Progress in Photovoltaics: Research and Applications,* 24(10), pp. 1332-1345.

Olson, J. M. et al., 1989. Ultralow recombination velocity at Ga0.5In0.5P/GaAs heterointerfaces. *Applied Physics Letters,* 55(12), pp. 1208-1210.

Paquette, B., Boucherif, A., Aimez, V. & Arès, R., 2016. Novel multijunction solar cell design for low cost, high concentration systems. *Progress in Photovoltaics: Research and Applications,* 24(2), pp. 150-158.

Pérez-Higueras, P., Ferrer-Rodríguez, J. P., Almonacid, F. & Fernández, E. F., 2018. Efficiency and acceptance angle of High Concentrator Photovoltaic modules: Current status and indoor measurements. *Renewable and Sustainable Energy Reviews,* Volume 94, pp. 143-153.

Phang, J. C. H., Chan, D. S. H. & Phillips, J. R., 1984. Accurate analytical method for the extraction of solar cell model parameters.. *Electronic Letters,* May, 20(10), pp. 406-408.

Picozzi, S., Asahi, R., Geller, C. B. & Freeman, A., 2002. Accurate First-Principles Detailed-Balance Determination of Auger Recombination and Impact Ionization Rates in Semiconductors. *Physical Review Letters,* 4 November, 89(19), pp. 197601 (1-4).

Pozner, R. et al., 2011. Vertical junction Si cells for concentrating. *Progress in Photovoltaics: Research and Applications,* 20(2), pp. 197-208.

Ritou, A., Voarino, P. & Raccurt, O., 2018. Does micro-scaling of CPV modules improve efficiency? A cell-to-module performance analysis. *Solar Energy,* Volume 173, pp. 789-803.

Rodrigo, P., Valera, A., Fernández, E. & Almonacid, F., 2019. Performance and economic limits of passively cooled hybrid thermoelectric generator-concentrator photovoltaic modules. *Applied Energy,* pp. 1150-1162.

Roulston, D., Arora, N. & Chamberlain, S., 1982. Modeling and measurement of minority-carrier lifetime versus doping in diffused layers of n+-p silicon diodes. *IEEE Transactions on Electron Devices,* Issue 29, pp. 284-291.

Sater, B. L. & Sater, N. D., 2002. *High voltage silicon VM solar cells for up to 1000 suns intensities.* s.l., s.n.

Schubert, E. F., 2006. *Light - Emitting Diodes.* Second Edition ed. s.l.:Cambridge University Press.

Segev, G. & Kribus, A., 2013. Performance of CPV modules based on vertical multi-junction cells under non-uniform illumination. *Solar Energy,* Volume 88, pp. 120-128.

Selberherr, S., 1984. *Analysis and Simulation of Semiconductor Devices..* s.l.:Springer-Verlag.

Shanks, K. et al., 2018. A >3000 suns high concentrator photovoltaic design based on multiple Fresnel lens primaries focusing to one central solar cell. *Solar Energy, 169, pp. 457-467,* Volume 169, pp. 457-467.

Siefer, G. & Bett, A. W., 2014. Analysis of temperature coefficients for III-V multijunction concentrator cells. *Progress in Photovoltaics: Research and Applications,* 22(5), pp. 515-524.

Silvaco, I., n.d. *Atlas User's Manual. Device Simulation Software.* s.l.:s.n.

Talavera, D. et al., 2016. A worldwide assessment of levelised cost of electricity of HCPV systems. *Energy Conversion and Management,* Volume 127, pp. 679-692.

Talavera, D. L., Perez-Higueras, P. J., Almonacid, F. & Fernández, E. F., 2017. A worldwide assessment of economic feasibility of HCPV power plants: Profitability and competitiveness. *Energy,* Volume 119, p. 408–424.

Theristis, M. & O'Donovan, T., 2015. Electrical-thermal analysis of III-V triple-junction solar cells under variable spectra and ambient temperatures. *Solar Energy,* Volume 118, pp. 533-546.

Tyukhov, I., 1996. Spectral-probe method of investigating solar cells.. *International conference "EuroSun'96", Proceedings, Germany, Verlag,* pp. 905-908.

Tyukhov, I. & Vasilev, A., 1995. Limiting efficiency of the ideal planar and edge-illuminated solar cells. *ISES Solar World Congress, Harare, Zimbabwe, Abstracts,* p. 74.

Valera, A., Fernández, E., Rodrigo, P. & Almonacid, F., 2019. Feasibility of flat-plate heat-sinks using microscale solar cells up to 10,000 suns concentrations. *Solar Energy,* Volume 181, pp. 361-371.

Vossier, A. et al., 2018. Performance bounds and perspective for hybrid solar photovoltaic/thermal electricity-generation strategies. *Sustainable Energy and Fuels,* 2(9), pp. 2060-2067.

Vurgaftman, I., Meyer, J. R. & Ram-Mohan, L., 2001. Band parameters for III-V compound semiconductors and their alloys. *Journal of Applied Physics,* 1 June, 89(11), pp. 5815-5875.

Wang, X. et al., 2013. Desing of GaAs Solar Cells Operating Close to the Shockley-Queisser Limit. *IEEE Jornal of Photovoltaics,* April, 3(2), pp. 737-744.

804 Wiesenfarth, M., Anton, I. & Bett, A., 2018. Challenges in the design of concentrator
805 photovoltaic (CPV) modules to achieve highest efficiencies. *Applied Physics Reviews,* 4(5), p.
806 art. no. 041601.

807 Xing, Y., 2013. Performance analysis of vertical multi-junction solar cell with front surface
808 diffusion for high concentration. *Solar Energy,* Volume 94, pp. 8-18.

809 Xing, Y. et al., 2015. A review of concentrator silicon solar cells. *Renewable and Sustainable*
810 *Energy Reviews,* Volume 51, pp. 1697-1708.

811 York, M. C. A. et al., 2018. Challenges and strategies for implementing the vertical epitaxial
812 heterostructure architechture (VEHSA) design for concentrated photovoltaic applications..
813 *Solar Energy Materials and Solar Cells ,* Volume 181, pp. 46-52.

814